Check for updates

ADVANCED FUNCTIONAL MATERIALS
www.afm-journal.de

Wireless, Battery-Free, Optoelectronic Diagnostic Sensor Integrated Colorimetric Dressing for Advanced Wound Care

Seokjoo Cho, Ji-Hwan Ha, Junseong Ahn, Hyeonseok Han, Yongrok Jeong, Sohee Jeon, Soonhyoung Hwang, Jungrak Choi, Yong Suk Oh, Dahong Kim, Su A Park, Donho Lee, Jihyeon Ahn, Byeongmin Kang, Byung-Ho Kang, Jun-Ho Jeong, and Inkyu Park**

Recently, addressing various wounds, ranging from skin injuries to pressure and chronic ulcers, has necessitated a more detailed approach to wound condition monitoring aimed at enhancing the patient's quality of life. Although most available wound dressings offer protection and promote the regeneration of wound lesions, they fail to monitor wound progression. To meet this need, this study introduces a pioneering solution: a wireless, battery-free, optoelectronic diagnostic sensor seamlessly integrated into a colorimetric, pH-sensitive wound dressing, designed to significantly enhance patient quality of life through improved wound care. Curcumin-polycaprolactone (C-PCL) dressing protect the wounds, promote cell regeneration, and possess antimicrobial properties. In addition, the dressing exhibits colorimetric pH-monitoring capabilities across different wound conditions, enabling individuals without specialized knowledge to assess the status of their wounds. The core innovation lies in the integration of a green light-emitting diode (LED) and photodiode, which meticulously evaluates color changes from yellow to red of colorimetric dressing, enhance the precision of this user-friendly colorimetric diagnosis strategy. The integration of wireless battery-free systems facilitates quantitative and real-time monitoring of wound data in patients without inconvenience. These innovations will pave the way for rapid wound status evaluation, ensuring timely interventions and optimized care for deteriorating wound conditions.

1. Introduction

Wound management has long been a crucial concern in healthcare, prompting a need for more comprehensive approaches to addressing a broad spectrum of wounds, ranging from common skin injuries to intricate conditions such as pressure ulcers and chronic ulcers.[1,2] Chronic wounds, characterized by inconsistent healing or necessitating delayed treatment, present formidable challenges and issues that demand attention. Numerous studies underscore the significance of effective chronic wound management. Primarily, chronic wounds often give rise to complications such as severe pain, inflammation, and infection, exacerbating patients' health status and complicating the healing process.[3,4] Consequently, chronic wounds significantly diminish patients' quality of life, imposing additional social and psychological burdens.[5–8] Furthermore, the treatment and management of chronic wounds incur substantial costs and escalate the utilization of healthcare resources, estimated between $28.1 to $96.8 billion.[9–11] Managing chronic wounds frequently entails intricate treatment procedures that necessitate close collaboration among medical staff and continuous monitoring. Moreover, the severity of chronic wounds is compounded by an aging population, with an estimated increase in chronic diseases exceeding 1.51 per 1000 population.[12,13] These demographic characteristics underscore the growing importance of chronic wound

S. Cho, J.-H. Ha, H. Han, D. Lee, J. Ahn, B. Kang, B.-H. Kang, I. Park
Department of Mechanical Engineering
Korea Advanced Institute of Science and Technology
Daejeon 34141, Republic of Korea
E-mail: inkyu@kaist.ac.kr

J.-H. Ha, S. Jeon, S. Hwang, D. Kim, S. A Park, B. Kang, B.-H. Kang, J.-H. Jeong
Nano Lithography and Manufacturing Research Center
Korea Institute of Machinery and Materials
Daejeon 34103, Republic of Korea
E-mail: jhjeong@kimm.re.kr

J. Ahn
Department of Electro-Mechanical Systems Engineering
Korea University
Sejong 30019, Republic of Korea

Y. Jeong
Korea Atomic Energy Research Institute (KAERI)
11, Daedeok-daero 989beon-gil, Yuseong-gu, Daejeon 34057, Republic of Korea

J. Choi
Electronics and Telecommunications Research Institute (ETRI)
Daejeon 34129, Republic of Korea

Y. S. Oh
Department of Mechanical Engineering
Changwon National University
Changwon 51140, Republic of Korea

The ORCID identification number(s) for the author(s) of this article can be found under https://doi.org/10.1002/adfm.202316196

DOI: 10.1002/adfm.202316196

 © 2024 Wiley-VCH GmbH

management, positioning it as a key challenge for future healthcare.

The main goals of wound management are to promote wound healing, to minimize complications, and to improve the patient's quality of life by closely monitoring the progress of the wound.[14] Chronic wound management requires monitoring factors related to infection and inflammation, accompanied by dressings that can protect the wound and promote healing. Additionally, it necessitates a smart monitoring system providing convenience to the patient and enabling specialized medical personnel to diagnose the patient's condition in real-time.[15] Traditional wound dressings have played a crucial role in protecting wounds and promoting healing, but they often had limitations in providing real-time monitoring of wound conditions.[16] Recently, many studies have focused on smart dressings capable of promoting wound healing, providing antimicrobial agents, and monitoring wound-related factors for patient monitoring.[17–19]

In chronic wound management, pH monitoring serves as an important indicator to assess wound progression, inflammation, infection, etc., providing optimal care to the patient.[20,21] During the wound healing process, the pH level changes, signifying the progression of the wound. As inflammation or infection advances in the tissue surrounding the wound, the pH level typically increases. The severity of the wound can elevate the pH level to as high as 9, and as the wound heals, the pH level decreases to a range of 6.5 to 5.5.[22,23] An increase or decrease in the pH level detected through pH monitoring provides information about inflammation, infection, or the progress of the healing process. Potentiometric[24–27] and colorimetric methods[28,29] have been used to monitor the pH level of chronic wounds. The potentiometric method quantitatively assesses the pH level of the wound but is limited by the poor biocompatibility and toxicity of the carbon materials-based electrode[30,31] and silver/silver chloride-based reference electrode,[32] which may result in DNA damage, cell death, and an increased risk of skin or organ cancers.[33,30] Conversely, colorimetric pH sensors can estimate the skin pH through the color change of a dressing-type sensor, enabling patients and caregivers to diagnose skin conditions and track wound progress without in-depth medical knowledge.[34,35] Additionally, wearable colorimetric pH sensors using biocompatible materials that promote the regeneration of wounded tissues have been proposed recently.[28,29,34,35] However, there is a limitation in quantitatively evaluating pH values based on the color changes by the wound healing, requiring a separate reference device. Therefore, there is a need for a platform that can be attached to the skin, allowing for real-time quantitative measurement of wound-related factors without causing discomfort to the patient.

Recent advances in wireless sensors for the real-time and quantitative measurement of physiological data at skin interfaces of patients support advanced approach to assessing the progression and healing trends of chronic wounds. Near-field communication (NFC)-based wireless sensor platforms are gaining attraction as optimal tools for wound diagnostics owing to their ability to provide real-time monitoring without batteries.[24,36–48] The proposed systems are designed for wearable applications, enabling the measurement of skin-related wound factors without causing discomfort to the patient. Furthermore, in addition to these trends, sensors that have the ability to not only monitor wound-related factors but also protecting the skin and promoting wound healing can be adequate devices for advanced wound management.

Our research aims to introduce an advanced approach to wound diagnostics through the use of colorimetric wound dressings with wireless, battery-free, optoelectronic diagnostic sensors. A wound dressing composed of curcumin and polycaprolactone-based composite material (C-PCL) serves the multifunctional purpose of protecting chronic wounds and promoting healing based on its antimicrobial properties. These dressings leverage curcumin's colorimetric pH-monitoring properties to visually identify various wound conditions, making them accessible to individuals lacking medical expertise. An optoelectronic-based diagnostic sensor, comprising a green light-emitting diode (LED) and a photodiode (PD), enables the quantitative measurement of color change of the curcumin from yellow to red. Integrated with an NFC system, these sensors are capable real-time and quantitative monitoring of patient wound status information. Additionally, this device enables wireless data communication and power supply without causing any inconvenience to patients' mobility. It is also convenient owing to its lightweight characteristics (5 g) and the absence of bulky batteries.

2. Results and Discussion

2.1. Research Concept

In order to improve wound management, this study proposes the development of a curcumin-based wound dressing and a wireless, battery-free optoelectronic diagnostic sensor. The dressing incorporates a color-altering mechanism activated by an increase in pH resulting from the dissociation of hydrogen atoms within curcumin molecule. A strategy for integrating an optoelectronic sensor, consisting of a green LED and a PD, to quantify color changes sets this approach apart from previous research on diagnostic dressings and patches that relied solely on curcumin-based color changes.[34] Furthermore, the NFC system is integrated into an optoelectronic sensor, facilitating wireless, and battery-free transmission of color data from the dressing. The combination of colorimetric wound dressing and NFC-based optoelectronic diagnostic sensor proposed in this study exhibits distinctive features compared to previously developed wound dressing methods and colorimetric dressings, including aspects such as color quantification and convenient diagnosis (Table S1, Supporting Information). **Figure 1** illustrates the research concept that depicts a colorimetric wound dressing accompanied by an NFC-based optoelectronic sensor. This advanced approach to wound care, capable of addressing diverse wound scenarios, including skin wound generation and the aggravation of chronic wounds, involves the utilization of a composite material, C-PCL, which contains curcumin and PCL. This composite is used in the fabrication of nanoscale fibers using an electrospinning process, resulting in a wound dressing capable of exhibiting color changes based on pH levels. The porous structure of the electrospun C-PCL nanofibers provides air permeability, and the presence of polyphenols in curcumin and the low surface energy properties of PCL enhance its antimicrobial properties. Owing to the slightly acidic nature of

© 2024 Wiley-VCH GmbH

16163028, 2024, 29, Downloaded from https://onlinelibrary.wiley.com/doi/10.1002/adfm.202316196 by Korea University Library, Wiley Online Library on [17/07/2024]. See the Terms and Conditions (https://onlinelibrary.wiley.com/terms-and-conditions) on Wiley Online Library for rules of use; OA articles are governed by the applicable Creative Commons License

16163028, 2024, 29, Downloaded from https://onlinelibrary.wiley.com/doi/10.1002/adfm.202316196 by Korea University Library, Wiley Online Library on [17/07/2024]. See the Terms and Conditions (https://onlinelibrary.wiley.com/terms-and-conditions) on Wiley Online Library for rules of use; OA articles are governed by the applicable Creative Commons License

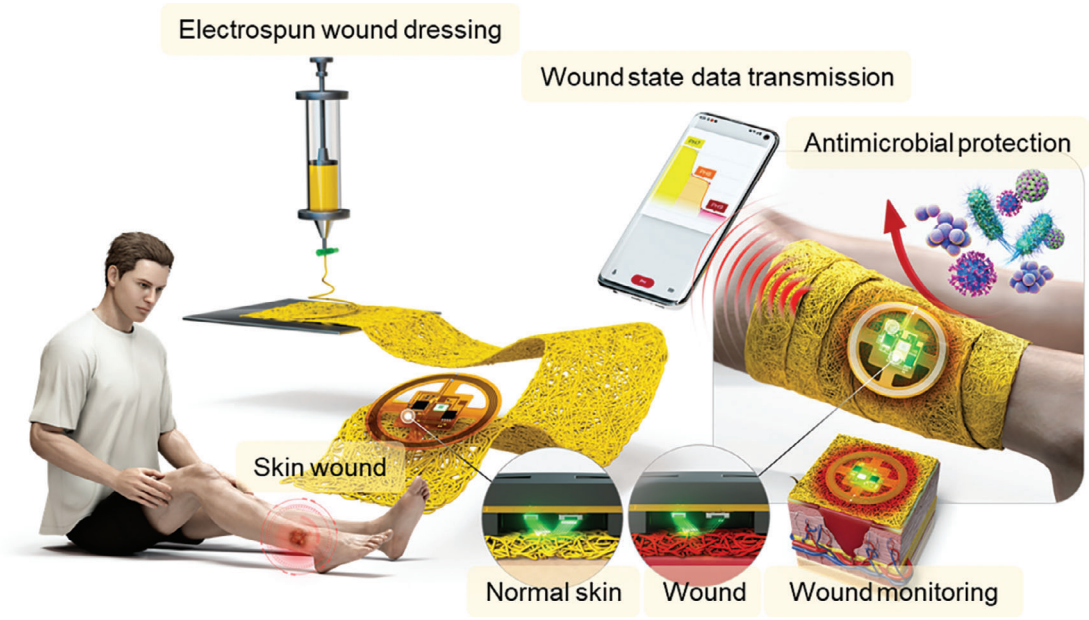


Figure 1. Research concept of colorimetric dressing, integrating green LED and PD-based diagnostic sensors, along with a near field communication (NFC) based wireless, battery-free system. The C-PCL composite nanofibers are fabricated by the electrospinning process. The affected area is then covered with C-PCL nanofiber sheets to monitor pH changes during the progression and degradation of wounds. Green LED and PD-integrated optoelectronic sensors are employed to detect color changes in this wound dressing as a response to varying pH levels. C-PCL dressings are also highly effective for wound protection because of their antimicrobial attributes, attributed to the polyphenols found in curcumin.

normal skin surfaces (pH 5.5–6),[20,21] C-PCL-based dressings exhibit a yellowish hue. When a wound develops or deteriorates, the pH level increases to approximately pH 8.5–9 due to endothelium exposure and exudate formation.[20] Consequently, a color change from yellow to red occurs, attributed to an alteration in the chemical structure of curcumin within the developed dressing. To quantify the yellow-to-red color changes, we designed an optoelectronic sensor relying on variations in the absorbance and reflectance of the PD signals. This sensor integrates a green LED to identify color shifts, particularly from yellow to red, securely affixed to a colorimetric dressing positioned on the wound lesion. The obtained color data can be wirelessly transmitted to a mobile device using the NFC system, enabling the diagnosis of lesion conditions.

2.2. Basic Characteristics of Electrospun C-PCL Nanofibers

The C-PCL fiber-based dressing, fabricated through electrospinning (Figure S1, Supporting Information), exhibited nanoscale diameters. **Figure** 2a displays scanning electron microscopy (SEM) images of the electrospun C-PCL nanofibers. The C-PCL fibers displayed a random orientation, with an average diameter of 416 nm and a standard deviation of 160 nm within the range of 200–800 nm (Figure 2b). The C-PCL dressings produced through the electrospinning process possess a randomly intertwined fiber structure, resulting in a superior air permeability attributed to their high porosity. Specifically, the electrospun C-PCL dressing demonstrated a significantly higher air permeability of 7.22 $cm^3\ cm^{-2}\ s^{-1}$ compared to the flat C-PCL film (0.05 $cm^3\ cm^{-2}\ s^{-1}$) (Figure S2, Supporting Information). These results are comparable to that of a commercial cotton (7.32 $cm^3\ cm^{-2}\ s^{-1}$) and surpass that of a denim fabric (3.41 $cm^3\ cm^{-2}\ s^{-1}$). The mechanical properties of the C-PCL dressing were assessed using a universal testing machine (UTM), with maximum stress, maximum strain, Young's modulus, and yield strength values measured at 5.33 MPa 514%, 0.21 MPa, and 1.48 MPa, respectively (Figure S3, Supporting Information). As shown in Figure 2c, Fourier transform infrared (FTIR) analysis was conducted to substantiate the composition of C-PCL, revealing the presence of an OH stretch (3400–3600 cm^{-1}) of curcumin within C-PCL, along with the identification of the alkaline chain (2945–2845 cm^{-1}) and C═O ester groups (1720 cm^{-1}) in PCL. To assess the biocompatibility and cell regeneration potential of the C-PCL dressing, a fibroblast growth experiment was conducted for 7 days. For comparison, a dressing composed of electrospun PCL fibers was fabricated, and its fibroblast proliferation performance was assessed under identical conditions. Consequently, the C-PCL dressing exhibited a remarkable 186% improvement in fibroblast growth compared to the PCL dressing, as shown in Figure 2d. This enhancement can be attributed to the multifunctional role of curcumin in wound healing, a well-known herbal material recognized for its anti-inflammatory,[49] antioxidant,[49,50] anticarcinogenic,[50] anticoagulant,[50] and antimicrobial properties,[51–53] all of which facilitate the cell proliferation. In Figure 2e, the morphological characteristics of fibroblast proliferation on the surfaces of both PCL and C-PCL dressings are depicted after 7 days, as observed by SEM. Furthermore, fibroblast cell proliferation morphologies were observed to be more uniform and widespread on the surface of the electrospun C-PCL dressing than on PCL dressing. The low surface energy (hydrophobic) of PCL inhibits microbial adsorption,

 © 2024 Wiley-VCH GmbH

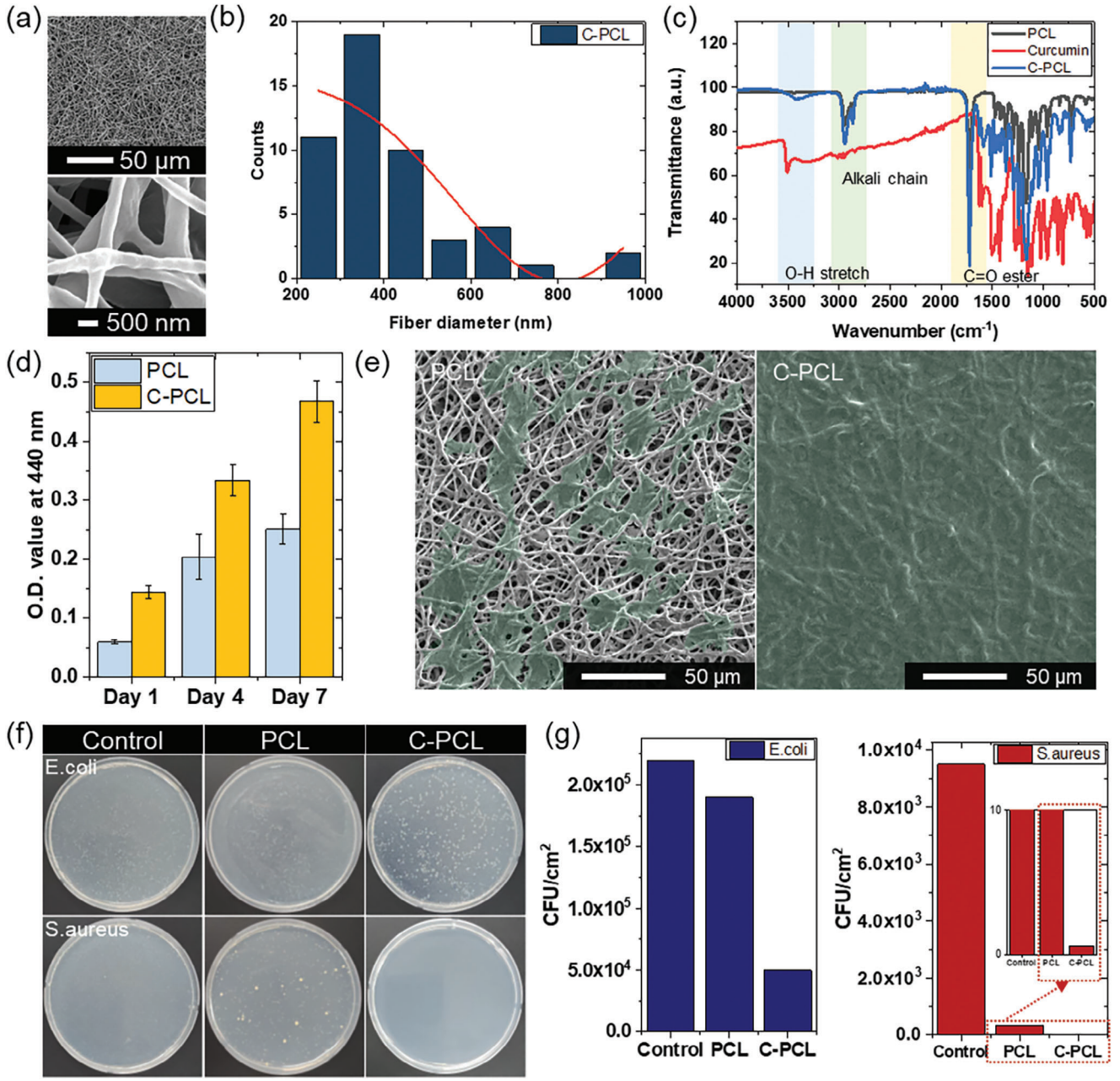


Figure 2. a) SEM image of electrospun C-PCL fibers. b) Distribution of electrospun C-PCL nanofiber diameters (average diameter: 416 nm, standard deviation: 160 nm, analysis area: 100 μm^2). c) FTIR analysis of PCL, curcumin, and C-PCL (OH stretching: 3400–3600 cm^{-1}, Alkali chain: 2945–2845 cm^{-1}, C=O ester: 1720 cm^{-1}). d) Results of fibroblast cell proliferation for electrospun PCL and C-PCL dressings over 7 days. e) SEM images showing the morphological characteristics of fibroblast cell proliferation on electrospun PCL and C-PCL dressings over 7 days. f) Photographs showing the results of the antimicrobial performance of electrospun PCL and C-PCL dressings against *E. coli* and *S. aureus*. g) Results of the antimicrobial tests performed on electrospun PCL and C-PCL dressings against *E. coli* and *S. aureus*.

whereas the substantial presence of curcumin, along with a significant number of polyphenols, confers antimicrobial properties that discourage microbial growth. An antimicrobial test was conducted on the gram-negative bacterium *Escherichia coli* (*E. coli*) and the gram-positive bacterium *Staphylococcus aureus* (*S. aureus*) according to the JIS Z 2801 standard to validate the antimicrobial properties of both PCL and C-PCL, as shown in Figure 2f. Against *E. coli*, the PCL dressing showed 13.6% antimicrobial activity compared to the only agar medium (control, 0% antimicrobial activity). In contrast, the C-PCL dressing displayed significantly enhancement of antimicrobial activity at 77.2% due to the presence of curcumin. For *S. aureus*, the PCL dressing demonstrated strong antibacterial activity at 96.5% when compared to the control group. Furthermore, the C-PCL dressing surpassed this, achieving an impressive 99.9% antimicrobial activity (Figure 2g).

© 2024 Wiley-VCH GmbH

16163028, 2024, 29, Downloaded from https://onlinelibrary.wiley.com/doi/10.1002/adfm.202316196 by Korea University Library, Wiley Online Library on [17/07/2024]. See the Terms and Conditions (https://onlinelibrary.wiley.com/terms-and-conditions) on Wiley Online Library for rules of use; OA articles are governed by the applicable Creative Commons License

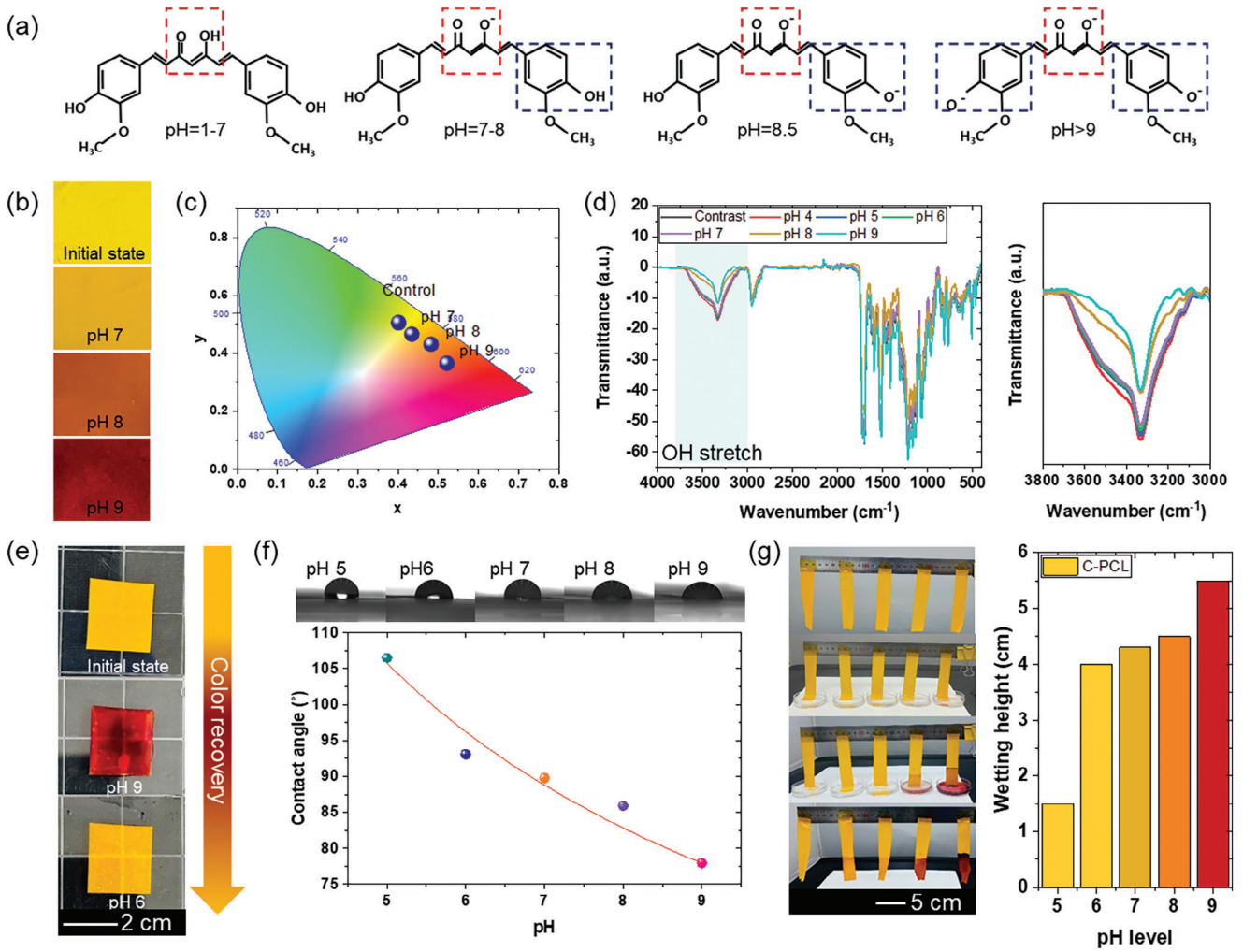


Figure 3. a) Schematic depiction of the alterations in curcumin chemical structure according to pH levels. b) Photograph showing the color change of electrospun C-PCL dressing in response to pH levels. c) Representation of the color of the C-PCL dressing in the CIE 1931 color space in relation to pH levels. d) FTIR analysis demonstrating the declining trend of hydroxyl groups within the curcumin chemical structure of C-PCL, attributed to the dissociation of hydrogen atoms as influenced by increasing pH levels. e) Photograph depicting the ability of C-PCL dressings to recover color and demonstrate reusability as pH levels change (red: pH 9, yellow: pH 6). f) Variations in the wettability of C-PCL in response to pH levels. The water contact angle decreased as the pH level increased. g) To assess the wettability of C-PCL dressings in relation to pH levels, a C-PCL strip of 10 cm in length (1 cm width) was fabricated, of which 1.5 cm was submerged in each pH buffer solution.

2.3. Colorimetric pH Sensing Performance of Electrospun C-PCL Dressing

Curcumin, a crucial component of electrospun C-PCL, displays notable characteristics wherein its color changes in response to shifts in both absorbance and reflectance, attributed to the dissociation/association of hydrogen atoms in curcumin-induced by varying pH levels.[54,55] **Figure 3a** illustrates the chemical structure of curcumin and its tendency to undergo hydrogen atom dissociation under varying pH levels. Figure S4 (Supporting Information) demonstrates the correlation between the color change of curcumin powder and the pH level, as indicated by the UV–vis spectroscopy changes in the pH buffer solution. The absorbance peak of the curcumin solution shifts from 424 nm at pH 9 to 420.7 nm at pH 5. Figure 3b depicts the change in color of the C-PCL dressing in response to varying pH levels, transitioning from an initial yellow state to dark yellow at pH 7, orange at pH 8, and red at pH 9. The color-change results of C-PCL, presented in the CIE 1931 color space (Figure 3c), illustrate the shift in color state from the yellow region to the red region as the pH level increases. Figure 3d presents findings from the FTIR analysis of the C-PCL dressing in different pH levels (pH 4–9). These results indicate that as the pH level increases, there is a reduction in the OH stretching band, attributed to the dissociation of hydrogen atoms, leading to a decline in the volume of the OH stretch within the range of 3400–3600 cm^{-1}. The color of the C-PCL dressing is expected to return to its original state as wound healing and relief are achieved. Hence, a color restoration experiment for the C-PCL dressing was conducted using buffer solutions at pH 9 and 6. Figure 3e shows the transformation of the C-PCL dressing, initially yellow, into red at pH 9, and its subsequent restoration from red to yellow

© 2024 Wiley-VCH GmbH

16163028, 2024, 29, Downloaded from https://onlinelibrary.wiley.com/doi/10.1002/adfm.202316196 by Korea University Library, Wiley Online Library on [17/07/2024]. See the Terms and Conditions (https://onlinelibrary.wiley.com/terms-and-conditions) on Wiley Online Library for rules of use; OA articles are governed by the applicable Creative Commons License

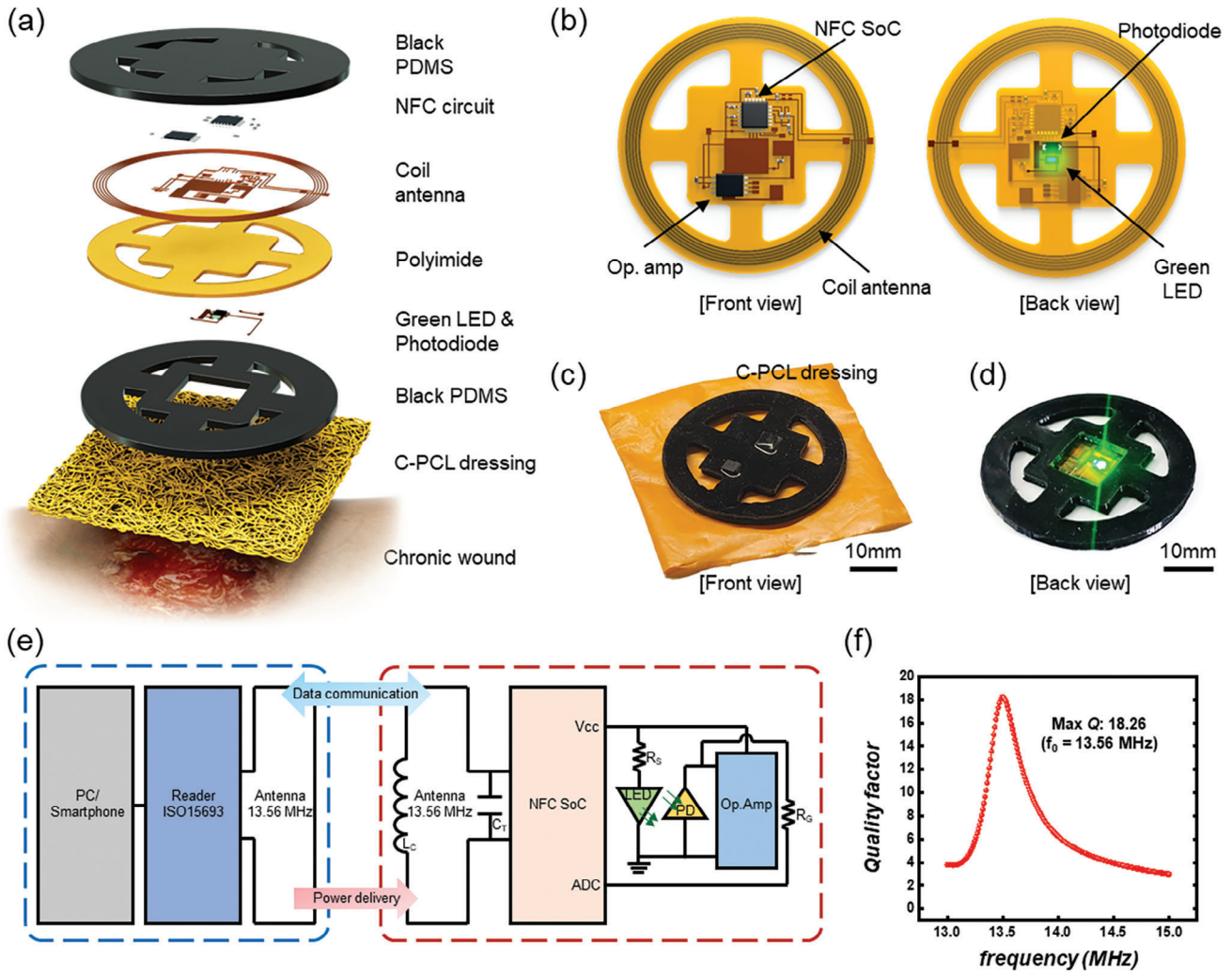


Figure 4. Schematics, photographs, and overview of a wireless, battery-free, optoelectronic diagnostic sensor. a) Extended-view schematic of a sensor with C-PCL dressing b) Schematic of the wireless patch that includes NFC circuit, green LED, photodiode, and chip electronics. c) Photograph of the wireless patch with a C-PCL dressing. d) Photograph of the optoelectronic sensor with green LED on e) Block diagram of the overall system. f) Quality factor of the device.

at pH 6 (Figure S5, Supporting Information). To verify the sensitivity and responsiveness to changing wound conditions, water contact angle (WCA) measurements were conducted at different pH levels. As depicted in Figure 3f, the WCA, initially 106.5° at pH 5, decreased with increasing pH, reaching 77.9° at pH 9 (pH 6: 93.1°, pH 7: 89.8°, and pH 8: 85.9°). This reduction was attributed to enhanced wettability resulting from alterations in the chemical structure of curcumin induced by an increase in pH.[56] The pH-dependent increase in wettability makes it well-suited for scenarios involving wound development and exacerbation, which typically involve an increase in pH levels. To further confirm the wettability, we cut C-PCL dressings to a length of 10 cm and immersed a specific portion (1.5 cm) in pH-specific buffer solutions, observing the point at which they became wet. As shown in Figure 3g, only 1.5 cm became wet in the pH 5 condition within 3 min, whereas at pH 6, 4 cm became wet, at pH 7, 4.3 cm became wet, at pH 8, 4.5 cm became wet, and at pH 9, 5.5 cm became wet. This trend, consistent with the previous WCA results, can be ascribed to the increased wettability of curcumin with increasing pH levels.

2.4. Design of Wireless, Battery-Free, Optoelectronic Diagnostic Sensor

Figure 4a presents an extended-view schematic of the wireless, battery-free, optoelectronic diagnostic sensor with a C-PCL dressing for pH monitoring in patients with chronic wounds. The sensor comprises an NFC circuit for wireless data communication and power supply, an optoelectronic component for pH monitoring, and polydimethylsiloxane (PDMS) packaging to prevent interference from external light and physical stimuli. In Figure 4b, a schematic of a flexible printed circuit board (fPCB) for wireless sensors is shown, including an NFC circuit and optoelectronic devices. Figure S6 and Table S2 (Supporting Information) describe the design and details of the electrical circuit and components of fPCB. The NFC circuit incorporates an NFC

© 2024 Wiley-VCH GmbH

16163028, 2024, 29, Downloaded from https://onlinelibrary.wiley.com/doi/10.1002/adfm.202316196 by Korea University Library, Wiley Online Library on [17/07/2024]. See the Terms and Conditions (https://onlinelibrary.wiley.com/terms-and-conditions) on Wiley Online Library for rules of use; OA articles are governed by the applicable Creative Commons License

system-on-chip (SoC), an operational amplifier (op-amp), and a coil antenna on the front side of a fPCB. The optoelectronic components, comprising a photodiode and a green LED for measuring the color change of the C-PCL dressing, are mounted on the back side of the fPCB. The fPCB is designed with holes between the coil and the circuit area to enhance breathability and allow biofluids from the dressing to pass through. In Figure 4c,d, photographs of the sensor patch packaged with black PDMS are depicted. The sensor patch is packaged in black PDMS for the electrical and physical stability of optoelectronics. The top packaging ensures stable data acquisition based on optoelectronic devices without the influence of external light sources, and the bottom packaging is perforated with a sensing part to secure the distance between the dressing and the optoelectronic device so that the light from the green LED can be reflected by the dressing and returned to the photodiode. The "Design and fabrication of the wireless, battery-free, and optoelectronic sensor" section of the "Methods" and Figure S7 (Supporting Information) illustrates the overall fabrication process of the sensor. The proposed dressing and wireless battery-free sensors can be employed and further advanced into diverse configurations to manage chronic wounds. Dressings can be attached or wrapped to effectively manage and diagnose chronic wounds of various shapes and sizes (Figure S8, Supporting Information). Figure 4e presents a block diagram of the overall operation of the device. The data acquisition circuit of the pH sensor, including the photodiode and op-amp, converts the current change under the difference in the reflection of green light, into an amplified voltage output. This value is passed on to the Analog-to-digital converters (ADCs) in the NFC SoC and stored in the chip memory. The coil antenna, coupled to the primary antenna and connected to a power module (NFC reader, smartphone), uses resonant magnetic inductive coupling for power harvesting at 13.56 MHz. Figure 4f shows the quality factor (Q) of the sensor, with a maximum Q of 18.26 at the antenna's resonant frequency (f_0 = 13.56 MHz). The power transfer efficiency η of the wireless sensor in the response frequency was calculated as 76% using Equation (1),[45] where k is the coupling efficient between the receiver antenna of the sensor and primary antenna of the NFC module, Q_n is the quality factor of the sensor (n = 1) and primary antenna (n = 2), and Z_{nm} is the impedance matrix elements between the sensor and primary antenna measured using a vector network analyzer. Additionally, Figure S9 (Supporting Information) shows that the power transfer efficiency and Q-factor of the wireless sensor were constant when the device was mounted on a human body. These results reveal that the power supply and data communication between the sensor and system do not depend on clothing or the human body.

$$\eta = \frac{k^2 Q_1 Q_2}{\left(1+\sqrt{1+k^2 Q_1 Q_2}\right)^2}, k = \frac{Im(Z_{21})}{Im(Z_{11})Im(Z_{22})}, Q_n = \frac{Im(Z_{nn})}{Re(Z_{nn})} \quad (1)$$

2.5. Working Mechanism and Characteristics of Optoelectronic Diagnostic Sensor

Figure 5a presents a cross-sectional view of the sensor, illustrating its working mechanism based on the color change of the dressing and the change in light reflection at different pH levels. The working mechanism of the sensor is the color perception based on variations in light reflection within specific wavelength ranges. The operation of this sensor relies on the principle that a color is determined by how it absorbs and reflects light. In the transition from yellow to red, the object becomes more efficient at absorbing shorter wavelengths, particularly green light, resulting in diminished green light reflection as the object shifts toward red. The green LED at the bottom of the NFC patch illuminates the C-PCL dressing, and the green light reflected from the dressing is detected using a photodiode. The color of the dressing changes from yellow to red as the pH of the chronic wound increased due to bacterial infection. The red shift of the C-PCL dressing reduces its reflectivity of green light, resulting in a decrease in the amount of light detected by the photodiode. Figure 5b shows the tendency of green light to reflect depending on the redness of the reflective surface. The color of an object determines which wavelengths of light it absorbs or reflects. A red object reflects wavelengths within the red spectrum and absorbs wavelengths of other colors, showing low reflectance of its complementary green light. Based on the CIELAB color space, a^* represents the redness of the color. Applying green light to a reference color sheet revealed a negative correlation between the a^* value of the color sheet and the green light reflection. Specifically, as the a^* value of the colored sheet increases, the reflection of green light decreases. Figure 5c illustrates the measurement of the reflected green light output as the dressing underwent a color change based on the pH, along with the a^* value measured using reference equipment. As the pH level increased, the dressing shifted toward redness, resulting in a corresponding increase in the measured a^* value. Notably, a concurrent decrease was observed in the reflection of green light (V_{out}) as the dressing shifted toward redness. While the color change exhibited by C-PCL dressings in response to blood from a wound lesion may raise concerns, it is important to note that the color of blood is blackish-red, distinct from the colors associated with pH 8 (orange) and pH 9 (red) environments. This distinction allows for effective differentiation using the optoelectronic diagnostic sensors (Figure S10, Supporting Information). In the unlikely event of a color change in this colorimetric dressing due to unexpected bleeding, the optoelectronic diagnostic sensor could be capable of detecting it and alerting the user to a bleeding condition. The C-PCL dressing must be capable of reacting to the minimum amount of biofluid from the wound lesion. To achieve this, the C-PCL dressing was exposed to a pH buffer solution equivalent to the minimum amount of biofluid droplets from the wound. Furthermore, when integrated with the C-PCL dressing, the optoelectronic diagnostic sensor effectively detects pH levels in a biofluid volume (125 µL min^{-1}) from the wound for the patch with an area of 25 mm × 60 mm (Figure S11, Supporting Information). The amount of biofluid was determined based on day 0, the initiation of the wound, as validated in previous studies employing a wound model on the back of a mouse.[57] Figure 5d,e shows the characteristics of the optoelectronic diagnostic sensor and the C-PCL dressing in different pH environments. Figure 5d shows stable and constant responses with negligible noise and drift during long-term monitoring (≈4 days) with constant pH of 7, 8, and 9, respectively. Figure 5e shows the voltage output of the sensor with a dressing that shifted its color at different pH levels from pH 7 to 9. To ensure stable operation of the sensor, it

© 2024 Wiley-VCH GmbH

16163028, 2024, 29, Downloaded from https://onlinelibrary.wiley.com/doi/10.1002/adfm.202316196 by Korea University Library, Wiley Online Library on [17/07/2024]. See the Terms and Conditions (https://onlinelibrary.wiley.com/terms-and-conditions) on Wiley Online Library for rules of use; OA articles are governed by the applicable Creative Commons License

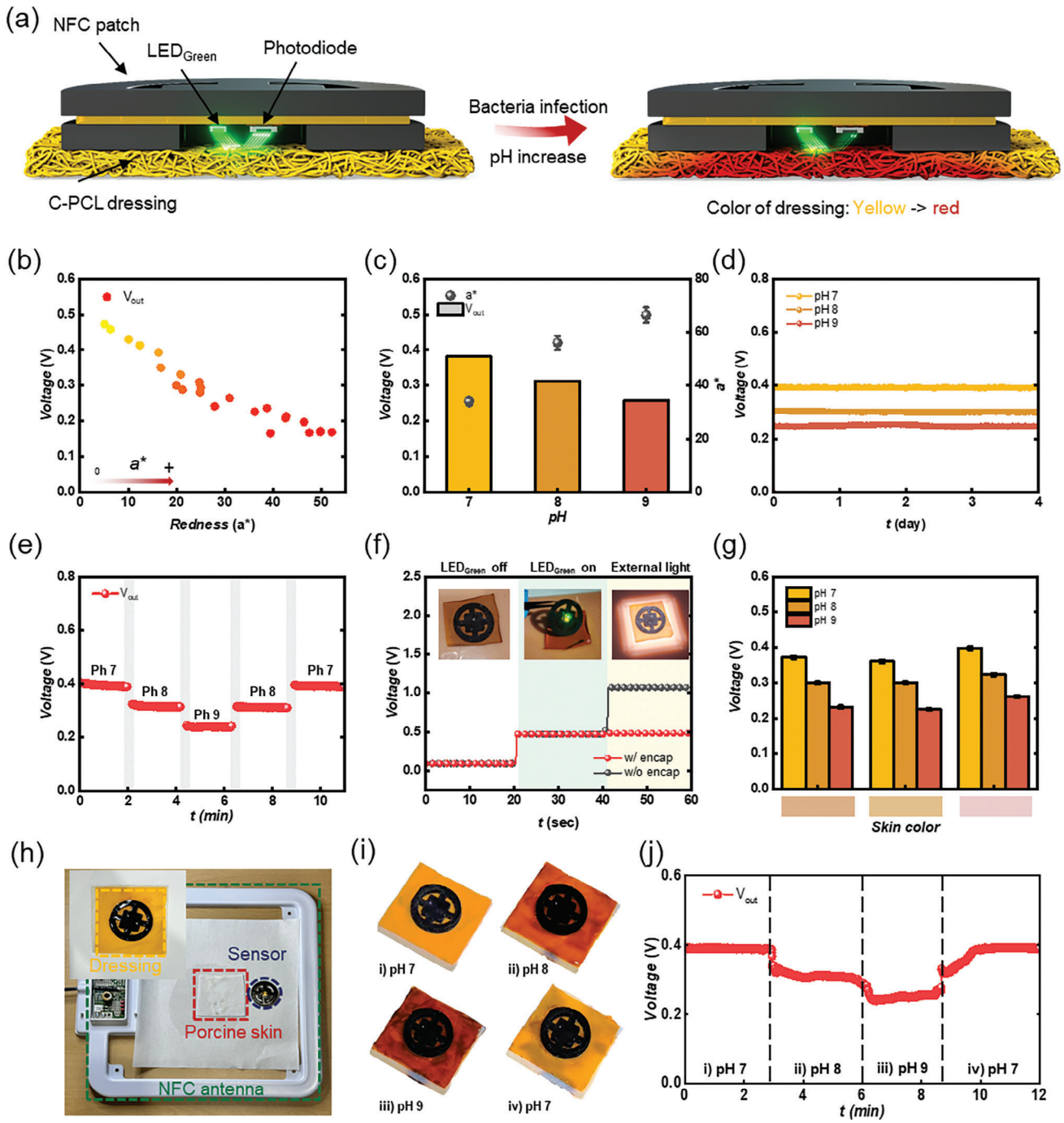


Figure 5. Working mechanism and performance characteristics of a wireless, battery-free, optoelectronic diagnostic sensor. a) Working mechanism of a sensor. b) Reflectance of a surface to green light among different redness (a^*) of an initially yellow sheet. c) Measurement of a^* and green light reflectance of C-PCL dressing. d) Voltage output of sensor with the C-PCL dressing under the constant pH levels of 7, 8, and 9, respectively, for 4 days. e) Voltage output of a sensor with the different pH levels of a C-PCL dressing. f) Voltage output of a sensor under the variation in external light. g) Voltage output of a sensor with the different skin colors. h) Photograph of an NFC sensing system with a porcine skin. i) Photographs of the wireless sensor with a C-PCL dressing and porcine skin. j) Voltage output of a sensor with a C-PCL dressing at the different pH levels.

© 2024 Wiley-VCH GmbH

16163028, 2024, 29, Downloaded from https://onlinelibrary.wiley.com/doi/10.1002/adfm.202316196 by Korea University Library, Wiley Online Library on [17/07/2024]. See the Terms and Conditions (https://onlinelibrary.wiley.com/terms-and-conditions) on Wiley Online Library for rules of use; OA articles are governed by the applicable Creative Commons License

is crucial for its response to remain consistent, regardless of external environmental factors. Figure 5f shows that the response of the sensor was influenced by the presence of the black PDMS packaging. When the sensor was exposed to an external light without black PDMS packaging, its response increased because of the impact of the external light. However, with the inclusion of PDMS packaging, the response of the sensor remained constant and unaffected by an external light. Furthermore, Figure 5g shows that the response of the sensor remained constant irrespective of the skin color beneath the dressing. This finding confirms that the performance of the sensor remains consistent regardless of the variations in a skin color when the dressing and sensor patch are applied to the skin. Figure S12 (Supporting Information) shows the morphological analysis of C-PCL fibers and voltage output of a wireless sensor with different diameters of C-PCL under varying pH conditions. The result indicates that the output signals obtained from the wireless sensors are stable with negligible differences, regardless of the diameter of electrospun C-PCL fibers. Figure 5h–j depicts the color changes observed in the C-PCL dressing and sensor when applied to a porcine skin, along with the corresponding variations in the sensor response as the pH levels change. When the pH was increased from 7 to 8, and subsequently to 9, the dressing transitioned to a reddish hue. Upon returning to the pH 7 environment, the dressing reversibly returned to its original yellow color (Figure 5i). This color alteration in response to pH was mirrored by changes in the electrical response of the sensor, which returned to its initial value upon reversion to pH 7. This demonstrates that the wireless battery-free sensor and dressing system offer both visual and electrical signals of pH changes. These wireless sensors and colorimetric pH dressings can be utilized in various application forms through integration with different antenna systems. Figure S13 (Supporting Information) illustrates the demonstration of powering the sensor via NFC with a smartphone, showcasing the system's compatibility with compact power sources for wearable applications. Moreover, by integrating with a fixed antenna integrated with a hospital bed, this setup can be enhanced for continuous monitoring of skin pH levels, particularly for special patient groups such as paralyzed patients who are susceptible to specific chronic wounds (e.g., pressure injuries). Figure S14 (Supporting Information) provides the demonstration of wireless sensor and C-PCL dressing with the NFC system integrated with a hospital bed. The two primary antennas integrated with a wood frame, foam mattress, and hospital bed allows the continuous monitoring of the full body of lying patient. Figure S14e (Supporting Information) shows the response of wireless sensor with the C-PCL dressing (control) that is attached on the right ankle. The result shows that the wireless sensor and dressing attached on the patient's right ankle provide a stable voltage output over time, allowing for continuous monitoring. Figure S15 (Supporting Information) demonstrates the attachment of the C-PCL dressing and wireless sensor to the skin, utilizing a medical film (1628 W, Tegaderm). The wireless sensor was mounted on top of the C-PCL dressing and secured in place with a medical film that is widely used in actual hospitals and numerous clinical trials.[58,59] After approximately 3 h of attachment, the sensor and dressing were removed, revealing no signs of allergic reactions on the skin (as shown in Figure S15b, Supporting Information). Additionally, Figure S16 (Supporting Information) shows the comparison of measured humidity level of the human skin using a commercial electronic device (IC-HSC001, Innoinsight) based on a bioelectrical impedance analysis. The healthy subjects (subject 1: male, 30-year-old; 78 kg; height, 173 cm; skin temperature ≈36 °C; subject 2: male, 25-year-old; 81 kg; height, 178 cm; skin temperature ≈36 °C) had a dressing and sensor attached to the skin for approximately 1 day. The results indicate that while the skin's humidity slightly increases with the application of the dressing, there is no significant difference in humidity levels before and after its application. (Change of humidity level (%) = 3% and 2% for subjects 1 and 2, respectively)

3. Conclusion

This paper introduced a wireless, battery-free, optoelectronic diagnostic sensor integrated with a colorimetric pH-responsive wound dressing, offering an advanced approach for managing chronic wounds. Our solution utilizes a composite material, C-PCL, combining curcumin and PCL, to create nanoscale fibers through electrospinning. The electrospun C-PCL nanofibers exhibit colorimetric pH monitoring properties through hydrogen atom dissociation and demonstrate antimicrobial properties owing to the presence of polyphenols in curcumin and the low surface energy characteristics of PCL. The combination of a C-PCL dressing and an optoelectronic sensor, consisting of a green LED and a PD, enables the real-time monitoring and quantification of the yellow-to-red color alteration in the C-PCL dressing at the wound site. The integration of wireless, battery-free systems with optoelectronics allows for the wireless communication of wound data to mobile devices, making it a convenient tool for individuals with chronic wounds. Moreover, a wireless and battery-free system enables patients to monitor wound conditions in real-time. This represents a significant advancement toward rapid wound status assessment, timely intervention, and optimized care for deteriorating wound conditions. Our research not only promises to improve the quality of life for patients with various types of wounds but also contributes to advancements in wound care technology. Anticipated benefits include empowering individuals, including patients and caregivers without a medical background, to manage wound conditions more effectively based on quantitative information. By enhancing convenience and facilitating real-time monitoring, our approach aims to alleviate the social and personal burdens associated with chronic wounds. Expanding research to measure other relevant factors, such as temperature, humidity, uric acid, and glucose for diagnosing chronic wounds, will clarify wound healing and deterioration aspects, expand our knowledge of wound care management, and improve diagnosis accuracy. While in this study, we developed a colorimetric dressing and wireless optoelectronic sensor specifically designed for the accurate diagnosis of diseases involving wounds and ulcers, our future goal is to fabricate a colorimetric diagnosable dressing integrated with additional optoelectronic sensors. These sensors will have the capability to monitor various factors, including sweat acidity, glucose, and lactic acid, for comprehensive disease state monitoring. Moreover, in subsequent studies, integrating auxiliary electronics such as low-dropout regulators can enhance the stability of the optical signal, consequently augmenting the precision of optical signal measurements.

© 2024 Wiley-VCH GmbH

16163028, 2024, 29, Downloaded from https://onlinelibrary.wiley.com/doi/10.1002/adfm.202316196 by Korea University Library, Wiley Online Library on [17/07/2024]. See the Terms and Conditions (https://onlinelibrary.wiley.com/terms-and-conditions) on Wiley Online Library for rules of use; OA articles are governed by the applicable Creative Commons License

4. Experimental Section

Materials: PCL (M_w = 80000) and curcumin were purchased from Sigma–Aldrich (USA). Dichloromethane and dimethylformamide (DMF) were obtained from Duksan Chemicals (Korea). Buffer solutions with varying pH levels were purchased from Duksan Chemicals.

Electrospun C-PCL Dressing Fabrication: The C-PCL solution was prepared using a magnetic stirring procedure. PCL was dissolved in a mixture of dichloromethane and DMF (1:1 v/v volume ratio) for 1 h, using a magnetic stirrer. Following this step, different quantities of curcumin (30 wt.% relative to the polymer) were added to the PCL solution, and an additional stirring process was conducted for 3 h. Subsequently, the C-PCL solution was sonicated to ensure the homogeneous dispersion of curcumin. The electrospinning process for the C-PCL nanofiber-based dressings was conducted by injecting the C-PCL solution at a rate of 1.5 mL h^{-1} with an input power of 21 kV. Electrospinning was carried out for 3 h, maintaining the electrospinning distance for C-PCL between the nozzle and target surface at 15 cm. The C-PCL dressing had a thickness of 100 µm and covered an area ranging from a minimum of 1 cm × 1 cm to a maximum of larger than 5 cm × 50 cm.

Material Characterization of Samples: The morphology of the electrospun C-PCL dressing and proliferating cells was examined using field-emission scanning electron microscopy (FE-SEM, Hitachi High-Technologies Corp, SU8230, Japan). FTIR analysis (range = 4000–400 cm^{-1}) was conducted with an FTIR spectrometer (Thermo Fisher Scientific, Nicolet iS50, USA). Mechanical properties of C-PCL were measured using the UTM. (AGS-X, Shimadzu) Water contact angle measurements were performed using contact angle measurement equipment (KRÜSS Scientific Equipment, Germany). The contact angle of C-PCL for each pH buffer solution was measured according to $\gamma_{SG} = \gamma_{SL} + \gamma_{LG} \cdot \cos(\theta_C)$ (Figure S17, Supporting Information). The color alteration of the electrospun C-PCL was observed using pH buffer solutions with different pH levels. To assess color distinction of C-PCL dressing using animal blood, The purchase and testing of horse blood (BIOZOA Biological Supply) were conducted.

Cell Proliferation: Human dermal fibroblast (HDF) cells were used for the cell proliferation test. The HDFs were cultured in Dulbecco's Modified Eagle's Medium–high glucose (DMEM; Gibco, USA) supplemented with 10% fetal bovine serum (FBS; R&D systems, USA) and 1% penicillin (Gibco, USA). The cells were maintained under condition of 37 °C with 5% CO_2. The medium was refreshed every 2 or 3 days.

WST-1 (Premix WST-1 Cell Proliferation Assay System; Takara, Japan) was used to measure mitochondrial dehydrogenase activity during the proliferation in the samples. The samples were immersed in ethanol for ≈1 min to disinfect them and then rinsed with Phosphate Buffered Saline (PBS) at least three times. The samples were air-dried on a clean bench, and ≈5 × 10^4 cells were seeded onto each sample to allow for cell adhesion, which was ensured over a period of >4 h. For samples with adherent cells, the extent of proliferation was assessed on days 1, 4, and 7. The WST-1 solution was prepared following the manufacturer's instructions. Subsequently, 250 µL of the solution was added to each sample and incubated for 45 min. Following incubation, 100 µL of supernatant from the reacted solution was extracted from a 96-well plate, and the absorbance was measured at a wavelength range of 440 nm using a microplate reader (SpectraMas iD3; Molecular Devices, USA).

SEM was employed to verify the cell adhesion morphology on the samples. After culturing cells for 7 days, the samples were rinsed with PBS, and the cells were fixed overnight in 4% paraformaldehyde. Subsequently, they underwent a dehydration process by immersing them sequentially in 10%, 30%, 50%, 70%, 90%, and 100% ethanol for 22485 min each.

Antimicrobial Performance: The antimicrobial efficacy against *E. coli* and *S. aureus* was assessed using the JIS Z 2801 standard method. Microorganism growth was supported by a liquid culture medium, specifically a nutrient agar plate consisting of Bacto-Peptone (5 g), beef extract (3 g), and distilled water (1000 mL). The nutrient agar was sterilized through autoclaving at 10^3 kPa and 120 °C. Microbes were cultivated in 10 mL of the nutrient agar medium at 37±1 °C for 24–48 h. Following this initial cultivation, the cells were further incubated for 18 h in a glass container, with three control test specimens and three processed samples. All flat media were incubated at 37±1 °C for 24–48 h. After incubation, the colonies in a Petri dish, containing between 30 and 300 colonies of probiotic water, were counted and recorded. To determine the number of live microbes (M), the formula M = Z×R×20 was applied, where Z represents the number of colonies, R signifies the dilution factor, and 20 represents the amount of saline used. The antimicrobial reduction rates were calculated using the formula log ($M_a - M_c$), where M_a stands for the initial control live microbial number, and M_c represents the live microbial number after 18 h of incubation.

Design and Fabrication of the Wireless, Battery-Free, and Optoelectronic Sensor: The sensor platform used a flexible printed circuit board (fPCB) processed by a direct UV laser ablation system (ProtoLaser U4, LPKF, USA) to yield the interconnect trace for the electronics. The NFC coil features an outer diameter (*dout*) of 34 mm, a wire diameter (*w*) of 0.25 mm, and a spacing between turns (*s*) of 0.1 mm, with a total of 5 turns (*n*). This configuration results in a self-inductance of 2.1 µH and an internal resistance of 3.26 Ω, coupled with a resonance capacitance of 66 pF, being similar with previous studies.[40,41,44,48] The circuit comprises various chip capacitors (C1–C7, Samsung Electro-Mechanics, South Korea) for filtering, a tuning capacitance (C8), chip resistors (RC0603 FR-07, Yageo, Taiwan), a green LED ($\lambda \approx$ 525 nm, Power consumption ≈ 2 mW, LT QH9G-Q2OO-25-2Z4Y, Osram Opto semiconductors, Germany), a photodiode (SFH2716, Osram Opto Semiconductors, Germany), an operational amplifier (ADA4505-2ARMZ, Analog Devices, USA), and an NFC SoC (RF430FRL152H, Texas Instruments, USA). (Figure S6 and Table S2, Supporting Information). Solder paste (SMDLTLFP10T5, ChipQuik, USA) was used to interconnect the surface-mounted components, including the NFC SoC and a micropower amplifier. Furthermore, soldering wire (SACX0307, Alpha Metal, USA) bonded the chip resistors and chip capacitors on the top of the fPCB, and a photodiode and a green LED on the bottom of the fPCB, respectively. The natural frequency of the coil antenna was set to 13.56 MHz by adjusting the tuning capacitor value and allowing communication with the primary antenna. The sensing platform was packaged with black polydimethylsiloxane (PDMS) layers on the top and bottom of the fPCB to protect the sensor platform from external light and physical stimuli. Although the bonding between polyimide and elastomer bonding is not good in general, sufficient mechanical bonding is formed through the sequential process of 10 min of plasma treatment (Cute-B, Femto Science, South Korea), liquid deposition of 1% (3-mercaptopropyl) trimethoxysilane (MPTMS, 95%, Sigma–Aldrich, USA) solution in methanol for 1 h, and epoxy resin.

Sensor Characterization: The characterization of the wireless sensor patch was carried out using an NFC reader and an antenna. Data communication and energy harvesting were made possible through the use of an antenna reader (ID ISC. LRM2500-A, FEIG Electronics, Germany), equipped with a primary antenna (ID IS. ANT310, FEIG Electronics, Germany) operating at a frequency of 13.56 MHz. The collected data were classified and visualized based on ISO 2018 software on the NFC protocol and customized Python code. Figure S18 (Supporting Information) shows the operating distance of wireless sensor from the center of primary antenna with different RF powers. The maximum available distance of transmission is 38.5 cm at the RF power of 12 W. Electrical analysis about the coil antenna of wireless sensor and primary antenna were conducted using a Vector Network Analyzer (TTR-500N, Tektronix) and an antenna analyzer (AA-230, Zoom). The wireless sensor had the resonance frequency at 13.563 MHz, with Return loss (RL) = 1.51 dB, Impedance (|Z|) = 41.02 Ω, and Phase = 101. 43°. Also, the primary antenna had the resonance frequency at 13.560 MHz, with RL = 23.87 dB, Impedance (|Z|) = 51.84 Ω, and Phase = 73.56°. As shown in Figure S19 (Supporting Information), both the wireless sensor and primary antenna have peak return loss near 13.56 MHz for the wireless, battery-free communication. Additionally, the redness of the reference color sheet and dressing was measured using a color meter (DSM Color Meter, Cortex Technology, Denmark).

NFC Protocol for Sensor: A radio-frequency identification (RFID) reader (TRF7970AEVM, Texas Instruments, USA) was utilized as an interface to control the writing process of the NFC System-on-a-Chip (SoC)

© 2024 Wiley-VCH GmbH

16163028, 2024, 29, Downloaded from https://onlinelibrary.wiley.com/doi/10.1002/adfm.202316196 by Korea University Library, Wiley Online Library on [17/07/2024]. See the Terms and Conditions (https://onlinelibrary.wiley.com/terms-and-conditions) on Wiley Online Library for rules of use; OA articles are governed by the applicable Creative Commons License

mounted on a flexible PCB. The interface between the RFID reader and the NFC SoC was established using a customized graphical user interface that adhered to the ISO 15 693 standard. This interface allowed control over the operation of the NFC SoC's operations. The NFC SoC was integrated with optoelectronics, data communication support, and wireless energy harvesting.

Demonstration and Characterization of Sensor with Human Subjects: The experiments with human subjects were approved by Institutional Review Board of Pusan National University Hospital (2111 017 109) and registered on the clinical research information service (CRIS, KCT0007094, Republic of Korea).

Supporting Information

Supporting Information is available from the Wiley Online Library or from the author.

Acknowledgements

S.C. and J.-H.H. contributed equally to this work. This work was supported by a National Research Foundation of Korea (NRF) grant funded by the Korean government (MSIT) Project Number: 2021R1A2C3008742); and the Technology Innovation Program (Development of Heterogeneous Multi-Sensor Micro-System Platform) funded By the Ministry of Trade, Industry & Energy (MOTIE, Korea) (Project Number: 00144157); Basic Research Program of Korea Institute of Machinery and Materials (KIMM), (Project Number: NK248B); and Alchemis Project grant funede by Korea Evaluation Institute of Industrial Technology (KEIT) & the Korea Government (MOTIE) (Project Number: 1415179744, 20019169).

Conflict of Interest

The authors declare no conflict of interest.

Data Availability Statement

The data that support the findings of this study are available from the corresponding author upon reasonable request.

Keywords

colorimetric pH dressing, curcumin composite, electrospinning, optoelectronic sensor, wireless sensor

Received: December 18, 2023
Revised: February 22, 2024
Published online: March 14, 2024

[1] G. Han, R. Ceilley, *Adv. Ther.* **2017**, *34*, 599.
[2] F. Werdin, M. Tenenhaus, H. O. Rennekampff, *Lancet.* **2008**, *372*, 1860.
[3] R. Zhao, H. Liang, E. Clarke, C. Jackson, M. Xue, *Int. J. Mol. Sci.* **2016**, *17*, 2085.
[4] D. Leaper, O. Assadian, C. E. Edmiston, *Br. J. Dermatol.* **2015**, *173*, 351.
[5] Y. Huang, B. Q. Mao, P. W. Ni, Y. Y. Shou, J. N. Ye, L. Hou, T. Xie, *Adv. Wound Care.* **2019**, *8*, 429.
[6] M. Olsson, K. Järbrink, U. Divakar, R. Bajpai, Z. Upton, A. Schmidtchen, J. Car, *Wound Repair Regener.* **2019**, *27*, 114.
[7] R. Yan, F. Yu, K. Strandlund, J. Han, N. Lei, Y. Song, *Wound Repair Regener.* **2021**, *29*, 70.
[8] M. H. Lentsck, T. Baratieri, M. R. Trincaus, A. P. Mattei, C. T. S. Miyahara, *Revista da Escola de Enfermagem.* **2018**, *52*, e03384.
[9] S. Kapp, N. Santamaria, *Int. Wound J.* **2017**, *14*, 1108.
[10] Z. J. Lo, X. Lim, D. Eng, J. Car, Q. Hong, E. Yong, L. Zhang, S. Chandrasekar, G. W. L. Tan, Y. M. Chan, S. C. Sim, C. W. Oei, X. Zhang, A. Dharmawan, Y. Z. Ng, K. Harding, Z. Upton, C. W. Yap, B. H. Heng, *Int. Wound J.* **2020**, *17*, 790.
[11] C. K. Sen, *Adv Wound Care.* **2019**, *8*, 39.
[12] W. Alam, J. Hasson, M. Reed, *J. Am. Geriatr. Soc.* **2021**, *69*, 2327.
[13] L. Martinengo, M. Olsson, R. Bajpai, M. Soljak, Z. Upton, A. Schmidtchen, J. Car, K. Järbrink, *Ann. Epidemiol.* **2019**, *29*, 8.
[14] E. Rezvani Ghomi, S. Khalili, S. Nouri Khorasani, R. Esmaeely Neisiany, S. Ramakrishna, *J. Appl. Polym. Sci.* **2019**, *136*, 1.
[15] N. Tang, Y. Zheng, D. Cui, H. Haick, *Adv. Healthcare Mater.* **2021**, *10*, 2101292.
[16] R. F. Pereira, P. J. Bártolo, *Adv. Wound Care.* **2016**, *5*, 208.
[17] S. Dhivya, V. V. Padma, E. Santhini, *BioMedicine.* **2015**, *5*, 24.
[18] M. Farahani, A. Shafiee, *Adv. Healthcare Mater.* **2021**, *10*, 2100477.
[19] R. Dong, B. Guo, *Nano Today.* **2021**, *41*, 101290.
[20] L. A. Schneider, A. Korber, S. Grabbe, J. Dissemond, *Arch. Dermatol. Res.* **2007**, *298*, 413.
[21] S. Schreml, R. M. Szeimies, S. Karrer, J. Heinlin, M. Landthaler, P. Babilas, *J. Eur. Acad. Dermatol. Venereol.* **2010**, *24*, 373.
[22] T. Cui, J. Yu, C. F. Wang, S. Chen, Q. Li, K. Guo, R. Qing, G. Wang, J. Ren, *Adv. Sci.* **2022**, *9*, 2201254.
[23] D. G. Metcalf, M. Haalboom, P. G. Bowler, C. Gamerith, E. Sigl, A. Heinzle, M. W. M. Burnet, *Wound Med.* **2019**, *26*, 100166.
[24] G. Xu, Y. Lu, C. Cheng, X. Li, J. Xu, Z. Liu, J. Liu, G. Liu, Z. Shi, Z. Chen, F. Zhang, Y. Jia, D. Xu, W. Yuan, Z. Cui, S. S. Low, Q. Liu, *Adv. Funct. Mater.* **2021**, *31*, 2100852.
[25] Y. Guo, X. Wei, S. Gao, W. Yue, Y. Li, G. Shen, *Adv. Funct. Mater.* **2021**, *31*, 2104288.
[26] M. Sharifuzzaman, A. Chhetry, M. A. Zahed, S. H. Yoon, C. I. Park, S. Zhang, S. Chandra Barman, S. Sharma, H. Yoon, J. Y. Park, *Biosens. Bioelectron.* **2020**, *169*, 112637.
[27] L. Vieira Jodar, L. O. Orzari, T. Storti Ortolani, M. H. M. T. Assumpção, F. C. Vicentini, B. C. Janegitz, *Electroanalysis.* **2019**, *31*, 2162.
[28] K. Zheng, Y. Tong, S. Zhang, R. He, L. Xiao, Z. Iqbal, Y. Zhang, J. Gao, L. Zhang, L. Jiang, Y. Li, *Adv. Funct. Mater.* **2021**, *31*, 2102599.
[29] J. H. Ha, Y. Jeong, J. Ahn, S. Hwang, S. Jeon, D. Kim, J. Ko, B. Kang, Y. Jung, J. Choi, H. Han, J. Gu, S. Cho, H. Kim, M. Bok, S. A. Park, J. H. Jeong, I. Park, *Mater. Horiz.* **2023**, *10*, 5983.
[30] N. A. Monteiro-Riviere, A. O. Inman, *Carbon.* **2006**, *44*, 1070.
[31] M. Uo, T. Akasaka, F. Watari, Y. Sato, K. Tohji, *Dent. Mater. J.* **2011**, *30*, 245.
[32] L. C. Clark, L. K. Noyes, R. B. Spokane, R. Sudan, M. L. Miller, S. Ertefai, D. A. Gough, S. C. Woodward, T. G. H. Yuen, W. F. Agnew, L. A. Bullara, A. M. Dymond, L. E. Kaechele, J. M. Jurist, P. H. J. Crandall, W. Neurosurg, Jackson, F. Duling, B. R. Tivol, W. F. Alvarez, R. B. Yuen, T. G. H. Velho, G. Froguel, P. Sternberg, R. Thevenot, D. R. Harrison, D. J. Turner, R. F. B. Baltes, H. P. Moussy, F. J. Harrison, et al., *Anal. Chem.* **1994**, *66*, 3528.
[33] R. Madannejad, N. Shoaie, F. Jahanpeyma, M. H. Darvishi, M. Azimzadeh, H. Javadi, *Chem. Biol. Interact.* **2019**, *307*, 206.
[34] J. H. Ha, J. Y. Kim, D. Kim, J. Ahn, Y. Jeong, J. Ko, S. Hwang, S. Jeon, Y. Jung, J. Gu, H. Han, J. Choi, G. Lee, M. Bok, S. A. Park, Y. S. Cho, J. H. Jeong, I. Park, *Adv. Mater. Technol.* **2023**, *8*, 2201765.

© 2024 Wiley-VCH GmbH

16163028, 2024, 29, Downloaded from https://onlinelibrary.wiley.com/doi/10.1002/adfm.202316196 by Korea University Library, Wiley Online Library on [17/07/2024]. See the Terms and Conditions (https://onlinelibrary.wiley.com/terms-and-conditions) on Wiley Online Library for rules of use; OA articles are governed by the applicable Creative Commons License

[35] B. Mirani, E. Pagan, B. Currie, M. A. Siddiqui, R. Hosseinzadeh, P. Mostafalu, Y. S. Zhang, A. Ghahary, M. Akbari, *Adv. Healthcare Mater.* **2017**, *6*, 10.
[36] J. W. Song, H. Ryu, W. Bai, Z. Xie, A. Vázquez-Guardado, K. Nandoliya, R. Avila, G. Lee, Z. Song, J. Kim, M.-K. Lee, Y. Liu, M. Kim, H. Wang, Y. Wu, H.-J. Yoon, S. Soo Kwak, J. Shin, K. Kwon, W. Lu, X. Chen, Y. Huang, G. A. Ameer, J. A. Rogers, *Sci. Adv.* **2023**,*9*, ade4687.
[37] N. T. Garland, J. W. Song, T. Ma, Y. J. Kim, A. Vázquez-Guardado, A. B. Hashkavayi, S. K. Ganeshan, N. Sharma, H. Ryu, M. K. Lee, B. Sumpio, M. A. Jakus, V. Forsberg, R. Kaveti, S. K. Sia, A. Veves, J. A. Rogers, G. A. Ameer, A. J. Bandodkar, *Adv. Healthcare Mater.* **2023**, *12*, 2301280.
[38] S. NajafiKhoshnoo, T. Kim, J. A. Tavares-Negrete, X. Pei, P. Das, S. W. Lee, J. Rajendran, R. Esfandyarpour, *Adv. Mater. Technol.* **2023**, *8*, 2201655.
[39] Y. Song, J. Min, Y. Yu, H. Wang, Y. Yang, H. Zhang, W. Gao, *Sci. Adv.* **2020**, *6*, 9842.
[40] S. Cho, H. Han, H. Park, S. U. Lee, J. H. Kim, S. W. Jeon, M. Wang, R. Avila, Z. Xi, K. Ko, M. Park, J. Lee, M. Choi, J. S. Lee, W. G. Min, B. J. Lee, S. Lee, J. Choi, J. Gu, J. Park, M. S. Kim, J. Ahn, O. Gul, C. Han, G. Lee, S. Kim, K. Kim, J. Kim, C. M. Kang, J. Koo, et al., *npj Flexible Electron.* **2023**, *7*, 8.
[41] S. Kim, Y. S. Oh, K. Lee, S. Kim, W. Y. Maeng, K. S. Kim, G. B. Kim, S. Cho, H. Han, H. Park, M. Wang, R. Avila, Z. Xie, K. Ko, J. Choi, M. Je, H. Lee, S. Lee, J. Koo, I. Park, *Small.* **2023**, *19*, 2206839.
[42] Y. Jiang, A. A. Trotsyuk, S. Niu, D. Henn, K. Chen, C. C. Shih, M. R. Larson, A. M. Mermin-Bunnell, S. Mittal, J. C. Lai, A. Saberi, E. Beard, S. Jing, D. Zhong, S. R. Steele, K. Sun, T. Jain, E. Zhao, C. R. Neimeth, W. G. Viana, J. Tang, D. Sivaraj, J. Padmanabhan, M. Rodrigues, D. P. Perrault, A. Chattopadhyay, Z. N. Maan, M. C. Leeolou, C. A. Bonham, S. H. Kwon, et al., *Nat. Biotechnol.* **2023**, *41*, 652.
[43] Z. Xiong, S. Achavananthadith, S. Lian, L. Edward Madden, Z. Xin Ong, W. Chua, V. Kalidasan, Z. Li, Z. Liu, P. Singh, H. Yang, S. P. Heussler, S. M. P. Kalaiselvi, M. B. H. Breese, H. Yao, Y. Gao, K. Sanmugam, B. C. K. Tee, P.-Y. Chen, W. Loke, C. Teck Lim, G. Shu Hui Chiang, B. Yeow Tan, H. Li, D. Laurence Becker, J. S. Ho, *Sci. Adv.* **2021**, *7*, 1617.
[44] H. Han, Y. S. Oh, S. Cho, H. Park, S. U. Lee, K. Ko, J. M. Park, J. Choi, J. H. Ha, C. Han, Z. Zhao, Z. Liu, Z. Xie, J. S. Lee, W. G. Min, B. J. Lee, J. Koo, D. Y. Choi, M. Je, J. Y. Sun, I. Park, *Small.* **2023**, *19*, 2205048.
[45] R. Lin, H. J. Kim, S. Achavananthadith, S. A. Kurt, S. C. C. Tan, H. Yao, B. C. K. Tee, J. K. W. Lee, J. S. Ho, *Nat. Commun.* **2020**, *11*, 1.
[46] S. Han, J. Kim, S. M. Won, Y. Ma, D. Kang, Z. Xie, K. T. Lee, H. U. Chung, A. Banks, S. Min, S. Y. Heo, C. R. Davies, J. W. Lee, C. H. Lee, B. H. Kim, K. Li, Y. Zhou, C. Wei, X. Feng, Y. Huang, J. A. Rogers, *Sci. Transl. Med.* **2018**, *10*, eaan4950.
[47] J. Kim, G. A. Salvatore, H. Araki, A. M. Chiarelli, Z. Xie, A. Banks, X. Sheng, Y. Liu, J. W. Lee, K. I. Jang, S. Y. Heo, K. Cho, H. Luo, B. Zimmerman, J. Kim, L. Yan, X. Feng, S. Xu, M. Fabiani, G. Gratton, Y. Huang, U. Paik, J. A. Rogers, *Sci. Adv.* **2016**, *2*, 1600418.
[48] Y. S. Oh, J.-H. Kim, Z. Xie, S. Cho, H. Han, S. W. Jeon, M. Park, M. Namkoong, R. Avila, Z. Song, S.-U. Lee, K. Ko, J. Lee, J.-S. Lee, W. G. Min, B.-J. Lee, M. Choi, H. U. Chung, J. Kim, M. Han, J. Koo, Y. S. Choi, S. S. Kwak, S. B. Kim, J. Kim, J. Choi, C.-M. Kang, J. U. Kim, K. Kwon, S. M. Won, et al., *Nat. Commun.* **2021**, *12*, 5008.
[49] V. Kant, A. Gopal, N. N. Pathak, P. Kumar, S. K. Tandan, D. Kumar, *Int. Immunopharmacol.* **2014**, *20*, 322.
[50] D. Akbik, M. Ghadiri, W. Chrzanowski, R. Rohanizadeh, *Life Sci.* **2014**, *116*, 1.
[51] M. Fallah, S. H. Bahrami, M. Ranjbar-Mohammadi, *J. Ind. Text.* **2016**, *46*, 562.
[52] M. R. Mohammadi, S. Rabbani, S. H. Bahrami, M. T. Joghataei, F. Moayer, *Mater. Sci. Eng. C.* **2016**, *69*, 1183.
[53] M. A. Olszewska, A. Gędas, M. Simões, *Food Res. Int.* **2020**, *134*, 109214.
[54] N. Pan, J. Qin, P. Feng, Z. Li, B. Song, *J. Mater. Chem. B.* **2019**, *7*, 2626.
[55] N. Pourreza, H. Golmohammadi, *Talanta.* **2015**, *131*, 136.
[56] T. Raja Sekharan, R. Margret Chandira, S. C. Rajesh, S. Tamilvanan, C. T. Vijayakumar, B. S. Venkateswarlu, *Biointerface Res. Appl. Chem.* **2021**, *11*, 14620.
[57] L. Shi, X. Liu, W. Wang, L. Jiang, S. Wang, *Adv. Mater.* **2019**, *31*, 1804187.
[58] L. B. Baker, J. B. Model, K. A. Barnes, M. L. Anderson, S. P. Lee, K. A. Lee, S. D. Brown, A. J. Reimel, T. J. Roberts, R. P. Nuccio, J. L. Bonsignore, C. T. Ungaro, J. M. Carter, W. Li, M. S. Seib, J. T. Reeder, A. J. Aranyosi, J. A. Rogers, R. Ghaffari, *Sci. Adv.* **2020**, *6*, 3929.
[59] C. K. Franz, N. K. Murthy, G. R. Malik, J. W. Kwak, D. D'Andrea, A. R. Wolfe, E. Farr, M. A. Stearns, S. Deshmukh, J. O. Tavee, F. Sun, K. N. Swong, L. Rydberg, R. J. Cotton, L. F. Wolfe, J. M. Walter, J. M. Coleman, J. A. Rogers, *J. Neuroeng. Rehabil.* **2022**, *19*, 108.

© 2024 Wiley-VCH GmbH

16163028, 2024, 29, Downloaded from https://onlinelibrary.wiley.com/doi/10.1002/adfm.202316196 by Korea University Library, Wiley Online Library on [17/07/2024]. See the Terms and Conditions (https://onlinelibrary.wiley.com/terms-and-conditions) on Wiley Online Library for rules of use; OA articles are governed by the applicable Creative Commons License